RSC Advances

PAPER

View Article Online
View Journal | View Issue

Check for updates

Cite this: *RSC Adv.*, 2020, **10**, 36734

Indirect-to-direct band gap transition and optical properties of metal alloys of $Cs_2Te_{1-x}Ti_xI_6$: a theoretical study

Diwen Liu,[ab] Wenying Zha,[c] Rusheng Yuan,[c] Benyong Lou*[d] and Rongjian Sa*[a]

Received 4th September 2020
Accepted 28th September 2020

DOI: 10.1039/d0ra07586h

rsc.li/rsc-advances

In recent years, double perovskites have attracted considerable attention as potential candidates for photovoltaic applications. However, most double perovskites are not suitable for single-junction solar cells due to their large band gaps (over 2.0 eV). In the present study, we have investigated the structural, mechanical, electronic and optical properties of the $Cs_2Te_{1-x}Ti_xI_6$ solid solutions using first-principles calculations based on density functional theory. These compounds exhibit good structural stability compared to $CH_3NH_3PbI_3$. The results suggest that Cs_2TeI_6 is an indirect band gap semiconductor, and it can become a direct band gap semiconductor with the value of 1.09 eV when the doping concentration of Ti^{4+} is 0.50. Moreover, an ideal direct band gap of 1.31 eV is obtained for $Cs_2Te_{0.75}Ti_{0.25}I_6$. The calculated results indicate that all the structures are ductile materials except for $Cs_2Te_{0.50}Ti_{0.50}I_6$. Our results also show that these materials possess large absorption coefficients in the visible light region. Our work can provide a route to explore stable, environmentally friendly and high-efficiency light absorbers for use in optoelectronic applications.

Open Access Article. Published on 19 1442. Downloaded on 08/04/46 01:03:44.
This article is licensed under a Creative Commons Attribution-NonCommercial 3.0 Unported Licence.

1. Introduction

Lead-based halide perovskites have attracted great attention for optoelectronic applications in the past ten years.[1–3] The power conversion efficiency (PCE) of lead-based halide perovskite solar cells increased to a high value of 25.2% in 2019.[4] However, the toxicity of lead and poor stability still remain significant challenges for commercial applications. Extensive efforts have been paid to exploring lead-free or lead-less and stable halide perovskite materials for solar cells. Sn^{2+} and Ge^{2+} metal ions have been expected to replace Pb^{2+} ions in perovskites.[5–9] Sn^{2+} ion is highly unstable and can be easily oxidized to Sn^{4+},[10] which results in decreased photovoltaic performance. To date, the highest PCE of Ge-based halide perovskites is only 4.94%.[11] Two dimensional (2D) layered perovskites have been also explored such as $A_3B_2X_9$ (A = Cs, Rb; B = Bi, Sb; X = I, Br, Cl).[12–17] However, these materials have large band gaps over 2.0 eV, which are not suitable for perovskite solar cells.

In recent years, halide double perovskites $A_2B^+B^{3+}X_6$ have been developed as stable and non-toxic alternatives to lead-based perovskite materials, where two toxic lead ions are substituted by using monovalent B^+ and trivalent B^{3+}, such as Ag^+, Bi^{3+}, and Sb^{3+}. Although most of the reported double perovskites show excellent stability, their band gaps are too large for application in single-junction solar cells.[18–21] A low band gap (1.66 eV) of double perovskites Cs_2NaBiI_6 has been synthesized, which possesses excellent stability and strong light absorption performance.[22] However, its PCE is only 0.42%, which is much lower than those of lead-based hybrid perovskites.

The vacancy-ordered double perovskites with formula of A_2BX_6 can be regarded as a derivative structure of the traditional ABX_3, where two toxic lead ions are substituted by one tetravalent ion to keep charge conservation as the conventional perovskites. Cs_2SnI_6 is one of the most representative perovskite materials, which belongs to a cubic structure with space group $Fm\bar{3}m$.[23] The previous study classified Cs_2SnI_6 as zero dimensional (0D) structure.[24] However, this compound still maintains three dimensional (3D) structure and presents 3D materials' properties, so it is still considered as 3D material.[25] Cs_2SnI_6 exhibits air and moisture stability, and strong visible light absorption, which are advantageous properties for photovoltaic applications.[26,27] The first tested solar cell using Cs_2SnI_6 as absorber material in air showed a small PCE of 0.96%.[26] Meanwhile, MA_2SnI_6 was found to have a direct band gap of 1.81 eV with a strong absorption coefficient of $\sim 7 \times 10^4$ cm^{-1}.[28]

[a]*Institute of Oceanography, Fujian Key Laboratory of Functional Marine Sensing Materials, Minjiang University, Fuzhou, Fujian 350108, China. E-mail: rjsa@mju.edu.cn*

[b]*College of Materials and Chemical Engineering, Pingxiang University, Pingxiang 337055, China*

[c]*State Key Laboratory of Photocatalysis on Energy and Environment, College of Chemistry, Fuzhou University, Fuzhou 350108, P. R. China*

[d]*Research and Testing Center of Pharmaceutical Formulations, Ocean College, Minjiang University, Fuzhou, Fujian 350108, P. R. China. E-mail: lby@mju.edu.cn*

This journal is © The Royal Society of Chemistry 2020

Open Access Article. Published on 19 1442. Downloaded on 08/04/46 01:03:44.
This article is licensed under a Creative Commons Attribution-NonCommercial 3.0 Unported Licence.

The material properties of $Cs_2Sn_{1-x}Te_xI_6$ were investigated to explore structure–property relationships with potential applications in photovoltaics.[29] In 2017, a promising family of all-inorganic based-Ti double perovskites were predicted to possess suitable band gaps, excellent optical absorption, and high stability.[30] In particular, the band gap of $Cs_2TiI_{6-x}Br_x$ can be tuned from 1.38 to 1.78 eV for single-junction and tandem solar cells.[30] A comprehensive and systematic study of halide perovskites has been performed by using density functional theory (DFT) calculations.[31] The theoretical study on the material properties of Cs_2TiX_6 (X = I, Br) has been investigated.[32–34] The PCE of 3.28% can be obtained for Cs_2TiBr_6 when it is incorporated into planar-heterojunction PSCs.[35] In 2018, Zhou *et al.* synthesized lead-free all-inorganic Cs_2PdBr_6 perovskite nanocrystals with a narrow band gap (1.69 eV) for the first time.[36] A series of lead-free Te-based double perovskites A_2TeX_6 (A = MA, FA, or BA; X = Br^- or I^-; MA = CH_3NH_3; FA = $CH(NH_2)_2$; BA = benzylamine) were reported to be potential materials for optoelectronic devices.[37] These Te-based double perovskites exhibited a tunable band gap, a low trap density, and a high mobility. Recently, the structural stability and electronic and optical properties of Te-based double perovskite materials were investigated by using first-principles calculations.[38] Therefore, the design of new non-/low-toxic stable halide perovskites for solar cells is inevitable.

In this work, the structural stability, mechanical properties, electronic and optical properties of double perovskites $Cs_2Te_{1-x}Ti_xI_6$ were investigated for the first time. The results show that $Cs_2Te_{0.50}Ti_{0.50}I_6$ has excellent stability, suitable direct band gap, and strong optical absorption, which is a promising candidate material for optoelectronic device. The mechanical properties of these materials are discussed in detail, and the results indicate that they are ductile materials except for $Cs_2Te_{0.50}Ti_{0.50}I_6$.

2. Computational details

First-principles calculations were performed by using Vienna *ab initio* simulation package (VASP).[39] The interaction between the core and valence electrons was described by the projector-augmented wave (PAW) method.[40] The generalized gradient approximation (GGA) of Perdew–Burke–Ernzerhof (PBE) was employed to describe the exchange–correlation functional.[41] A plane-wave energy cutoff of 500 eV was used. A $4 \times 4 \times 4$ *k*-point grid was adopted for geometric optimization until the convergence criteria of energy and forces were set to be 10^{-5} eV and 0.01 eV $Å^{-1}$, respectively. The structures were fully relaxed without any constraints. A denser $8 \times 8 \times 8$ *k*-point grid was employed for electronic and optical properties calculations. Four *k*-points *X* (0.5, 0, 0), *R* (0.5, 0.5, 0.5), *M* (0.5, 0.5, 0), and *G* (0, 0, 0) were selected for the bandgap calculations. In order to gain accurate lattice parameters of the studied systems, the van der Waals (vdW) interactions were adopted within vdW-DFT in all calculations.[42] For Cs_2TiI_6, considering the underestimation of the band gap in the standard DFT calculation, we used the DFT+U method[43] to obtain accurate electronic structure. Various values of *U* have been tested for Ti 3d orbitals of Cs_2TiI_6. $U = 2$ eV was finally chosen for the electronic and optical calculations for the $Cs_2Te_{1-x}Ti_xI_6$ solid solutions.

3. Results and discussion

3.1 Structure properties

The crystal structures of both Cs_2TeI_6 and Cs_2TiI_6 belong to the cubic phase with space group $Fm\bar{3}m$.[29,30] The calculated lattice constant of Cs_2TeI_6 is 11.66 Å, which is in good agreement with experimental value (11.71 Å).[29] The corresponding lattice constant of Cs_2TiI_6 is predicted to be 11.38 Å, which is much lower than its experimental value (11.67 Å).[30] The ion radii of Te^{4+} and Ti^{4+} are 0.97 Å and 0.61 Å, respectively. Interestingly, the experimental lattice constants of Cs_2TeI_6 and Cs_2TiI_6 are almost the same. It should be noted that the lattice parameter of Cs_2TiI_6 is estimated to be 11.67 Å according to the experimental XRD results. The optimized structures of the $Cs_2Te_{1-x}Ti_xI_6$ solid solutions are depicted in Fig. 1. *x* is the concentration of Ti^{4+}. The *x* values of 0.00, 0.25, 0.50, 0.75, and 1.00 are adopted in this study. For the species with $x = 0.25$, 0.50, and 0.75, all the possible arrangements are considered in this work. The results show that different structures with the same doping percentage

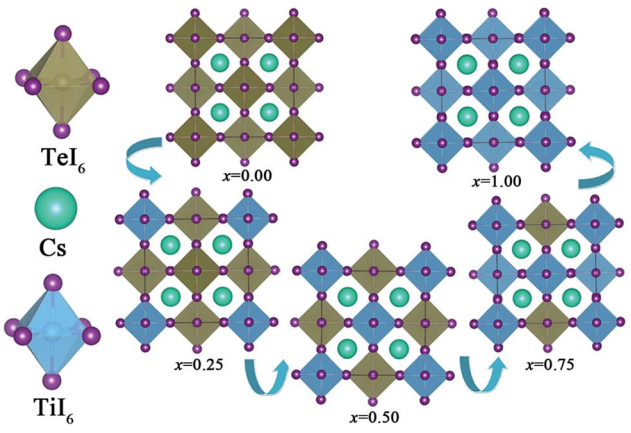

Fig. 1 The optimized structures of the $Cs_2Te_{1-x}Ti_xI_6$ solid solutions.

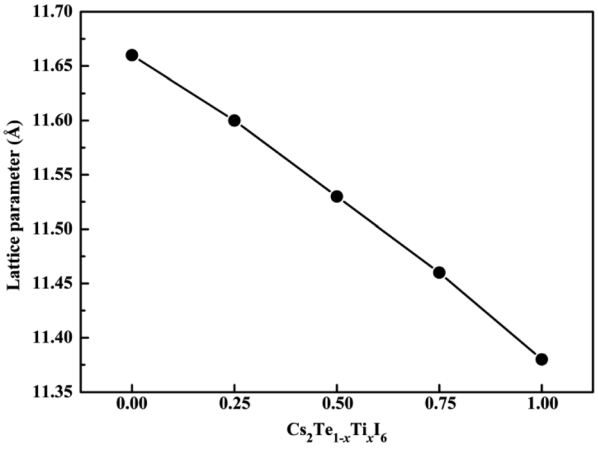

Fig. 2 The lattice constants of the $Cs_2Te_{1-x}Ti_xI_6$ solid solutions.

Open Access Article. Published on 19 1442. Downloaded on 08/04/46 01:03:44 .
This article is licensed under a Creative Commons Attribution-NonCommercial 3.0 Unported Licence.

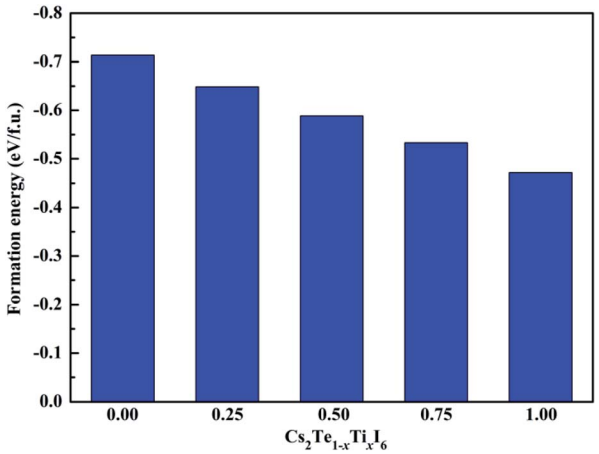

Fig. 3 Calculated formation energies of the $Cs_2Te_{1-x}Ti_xI_6$ solid solutions.

have the same stability, with calculated energy differences within less than 2 meV. The lattice constant of $Cs_2Te_{1-x}Ti_xI_6$ decreases gradually when the concentration of Ti^{4+}, as shown in Fig. 2. Moreover, the bond length Te–I (2.96 Å) of Cs_2TeI_6 is larger than the bond length Ti–I (2.76 Å) of Cs_2TiI_6.

The tolerance factor (t) has been widely used to predict the structural stability of perovskite material. The formula is defined as follows:[44]

$$t = \frac{R_A + R_X}{\sqrt{2}(R_B + R_X)} \quad (1)$$

where R_A, R_B, and R_X are the effective ionic radii for A, B, and X, respectively. In general, the perovskite structure is stable when the t value is in the range of 0.81–1.11.[45] Our calculated values of t are 0.86 and 0.97 for Cs_2TeI_6 and Cs_2TiI_6, respectively. These results confirm that the substitution of Ti^{4+} for Te^{4+} in Cs_2TeI_6 is feasible. To further assess the thermodynamic stability of the $Cs_2Te_{1-x}Ti_xI_6$ solid solutions, we have calculated their formation energies. The formation energy can be obtained according to the following equation:

$$\Delta H = \Delta E(Cs_2Te_{1-x}Ti_xI_6) - 2\Delta E(CsI) - (1 - x)\Delta E(TeI_4) - x\Delta E(TiI_4) \quad (2)$$

where $E(Cs_2Te_{1-x}Ti_xI_6)$, $E(CsI)$, $E(TeI_4)$, and $E(TiI_4)$ are the total energy of $Cs_2Te_{1-x}Ti_xI_6$, CsI, TeI_4, and TiI_4, respectively. The calculated formation energies of the $Cs_2Te_{1-x}Ti_xI_6$ solid solutions are demonstrated in Fig. 3. Our calculated result shows that the ΔH value of $MAPbI_3$ is 0.01 eV per f.u., which is in good agreement with the previous reported data.[46] These results indicate that $MAPbI_3$ is marginally stable. It can be seen that all the compounds exhibit good stability with larger negative ΔH values compared to $MAPbI_3$. Moreover, it is observed that the structural stability of $Cs_2Te_{1-x}Ti_xI_6$ decreases gradually with the increasing concentration of Ti^{4+}. In addition, the phonon spectrum of the mixed-metal double perovskites are also studied. As shown in Fig. 4, it can be seen that none of the imaginary phonon mode exists for $Cs_2Te_{0.75}Ti_{0.25}I_6$ and $Cs_2Te_{0.25}Ti_{0.75}I_6$, which indicate that they are kinetically stable. Interestingly, $Cs_2Te_{0.50}Ti_{0.50}I_6$ has very small imaginary frequencies. According to the previous study,[47] all small imaginary frequencies will disappear when it is at room temperature. Therefore, $Cs_2Te_{0.50}Ti_{0.50}I_6$ is considered to be a stable structure at room temperature.

3.2 Mechanical properties

To predict the mechanical stability of double perovskite $Cs_2Te_{1-x}Ti_xI_6$, the corresponding elastic constants were calculated

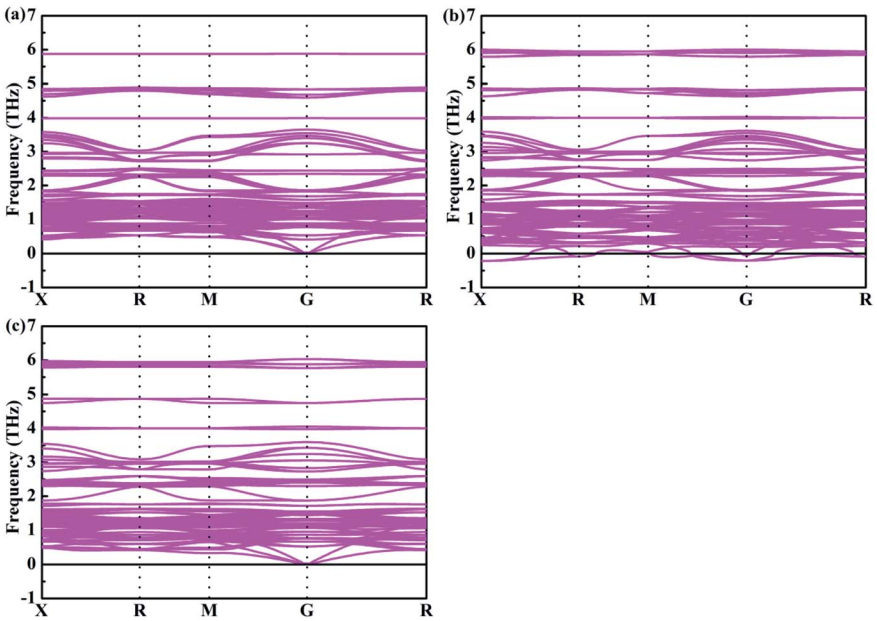

Fig. 4 Phonon spectrum of (a) $Cs_2Te_{0.75}Ti_{0.25}I_6$, (b) $Cs_2Te_{0.50}Ti_{0.50}I_6$, and (c) $Cs_2Te_{0.25}Ti_{0.75}I_6$.

 This journal is © The Royal Society of Chemistry 2020

Open Access Article. Published on 19 1442. Downloaded on 08/04/46 01:03:44 .
This article is licensed under a Creative Commons Attribution-NonCommercial 3.0 Unported Licence.

Table 1 The calculated elastic constants C_{ij} (GPa), bulk modulus B (GPa), shear modulus G (GPa), Young's modulus (E), Pugh's ratio (B/G), and Poisson's ratio ν of $Cs_2Te_{1-x}Ti_xX_6$

	C_{11}	C_{12}	C_{44}	B	G	E	B/G	ν
Cs_2TeI_6	19.14	10.24	8.78	13.21	6.68	17.16	1.98	0.28
$Cs_2Te_{0.75}Ti_{0.25}I_6$	20.20	9.80	9.86	13.27	7.63	19.20	1.74	0.26
$Cs_2Te_{0.50}Ti_{0.50}I_6$	17.51	8.39	9.98	11.43	7.29	18.03	1.57	0.24
$Cs_2Te_{0.25}Ti_{0.75}I_6$	19.14	11.08	10.27	13.77	7.06	18.08	1.95	0.28
Cs_2TiI_6	17.85	10.29	10.70	12.81	7.05	17.88	1.82	0.27

using the finite strain theory.[48] For cubic structure, the Born stability criteria is given as follows:[49]

$$C_{11} - C_{12} > 0,\ C_{11} + 2C > 120,\ C_{44} > 0 \quad (3)$$

The calculated results of three independent elastic constants are listed in Table 1. All the compounds satisfy the above Born stability criteria, indicating that they are mechanical stable. The bulk modulus (B) and shear modulus (G) can be obtained by using Hill approximations.[50] The Young's modulus (E) and Poisson ratio (ν) can be calculated from the values of bulk modulus and shear modulus by applying the following formula:[51]

$$E = 9BG/(3B + G),\ \nu = (3B - 2G)/(6B + 2G) \quad (4)$$

In order to investigate the ductility and brittleness of the studied double perovskites, we calculated the Pugh's and Poisson ratios. The Pughs's ratio is the ratio between bulk modulus and shear modulus (B/G), which is proposed by Pugh.[52] The material is considered as ductile when the value of Pugh's ratio is larger than 1.75, otherwise it is brittle. The Poisson's ratio can also be used to separate the ductile materials from brittle materials. The ductile materials have the Poisson's ratio greater than 0.26, and it is smaller than 0.26 for brittle materials.[53] From Table 1, it can be seen that $Cs_2Te_{0.50}Ti_{0.50}I_6$ is a brittle material, while other four compounds are ductile materials. It should be noted that the Poisson's ratio values of the studied double perovskites are close to the required lowest limit. The smaller the value of Young's modulus, the better flexibility of a material. The results show that Young's modulus of Cs_2TeI_6 is the smallest among the five structures, which indicates that it is

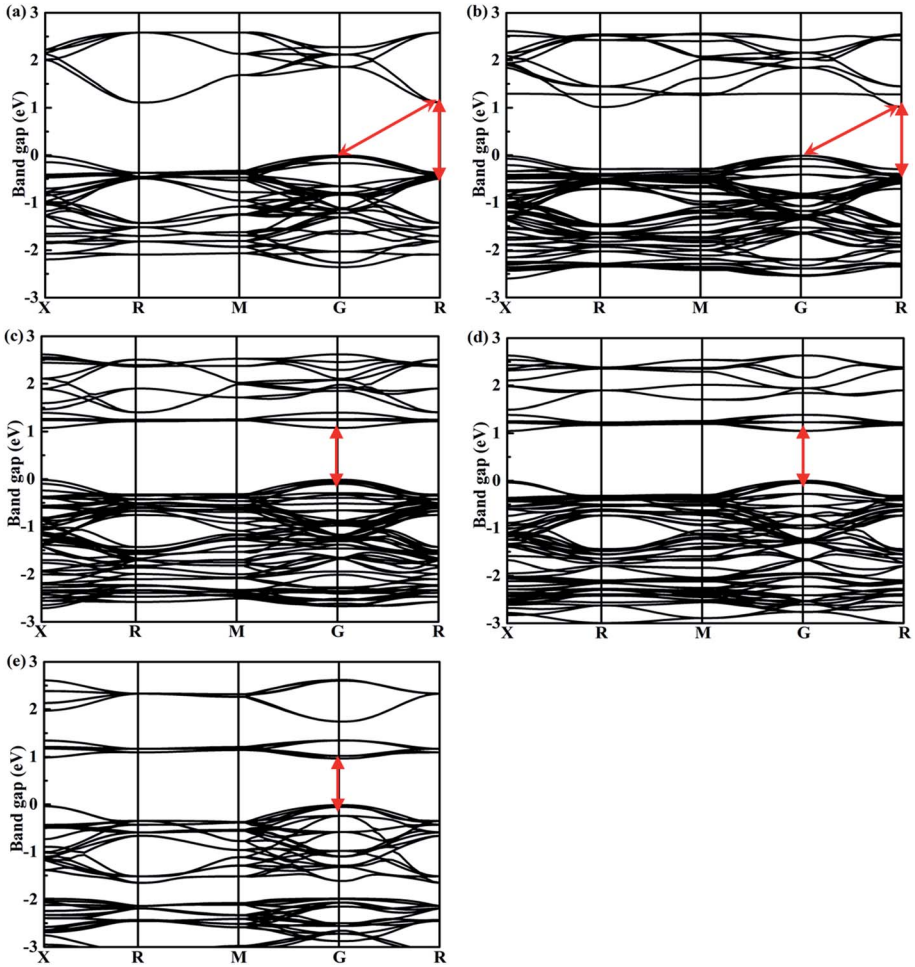

Fig. 5 Calculated band structures of double perovskites along the X–R–M–G–R path for (a) Cs_2TeI_6, (b) $Cs_2Te_{0.75}Ti_{0.25}I_6$, (c) $Cs_2Te_{0.50}Ti_{0.50}I_6$, (d) $Cs_2Te_{0.25}Ti_{0.75}I_6$, and (e) Cs_2TiI_6.

Open Access Article. Published on 19 1442. Downloaded on 08/04/46 01:03:44 .
This article is licensed under a Creative Commons Attribution-NonCommercial 3.0 Unported Licence.

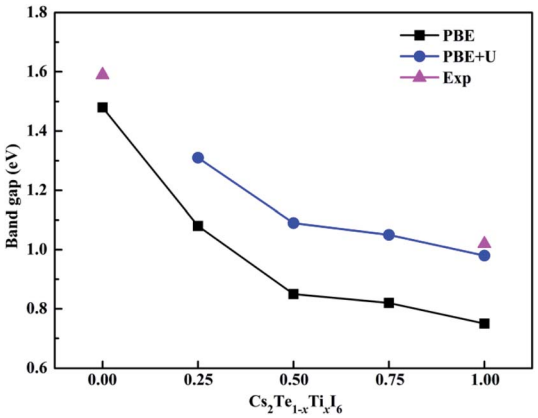

Fig. 6 Experimental and theoretical band gap trends with different methods of $Cs_2Te_{1-x}Ti_xI_6$.

the most flexible. Moreover, it is beneficial to form high quality film for ductile materials.

3.3 Electronic properties

The band structures calculated along high symmetry directions in the Brillouin zone are shown in Fig. 5. Cs_2TeI_6 has an indirect band gap between *G* and *R* point, and a direct band gap at *R* point. The indirect and direct band gaps of Cs_2TeI_6 are 1.12 and 1.48 eV, respectively. The previous reported band gap of Cs_2TeI_6 is about 1.5 eV,[54,55] and the recent experimentally observed optical gap is 1.59 eV.[29] The band gap of Cs_2TiI_6 with the PBE method is 0.75 eV, which is lower than its experimental value (1.02 eV).[30] Therefore, the DFT+U method is employed to obtain accurate band gap of Cs_2TiI_6. The result shows that Cs_2TiI_6 possesses a direct band gap with 0.98 eV at the *G* point, which is in good agreement with its experimental value.[30] The Spin–orbit coupling (SOC) effect on the electronic structures of Te- and Ti-based perovskites is small.[30,37] It is observed that $Cs_2Te_{0.50}Ti_{0.50}I_6$ is a direct band gap semiconductor with the value of 1.09 eV, while $Cs_2Te_{0.75}Ti_{0.25}I_6$ is an indirect band gap semiconductor. The direct band gap of $Cs_2Te_{0.25}Ti_{0.75}I_6$ is 1.05 eV. The trend in band gap is displayed in Fig. 6. The band gap of Cs_2TeI_6 reduces gradually when the ratio of Ti^{4+} increases. The band gaps of the two calculations with PBE and PBE+U show the same tendency. The variation in band gap is only 0.11 eV when the concentration of Ti^{4+} changes from 0.50 to 1.00. It should be noted that the direct band gap of Cs_2TeI_6 is close to the experimental value. The direct band gap of $Cs_2Te_{0.75}Ti_{0.25}I_6$ is 1.31 eV, which is a potential candidate for single-junction solar cells according to the Shockley–Queisser theory.[56] An indirect-to-direct band gap transition can be observed when the doping content of Ti^{4+} increases from 0.25 to 0.50. Moreover, the direct band gap is significantly reduced by 0.22 eV. It can be seen that the band gaps of the $Cs_2Te_{1-x}Ti_xI_6$ solid solutions are apparently underestimated at the PBE method, as shown in Fig. 6.

Fig. 7 shows the calculated density of states of the $Cs_2Te_{1-x}Ti_xI_6$ solid solutions. For Cs_2TeI_6, the valence band maximum (VBM) is mainly contributed by the I-p orbitals, while

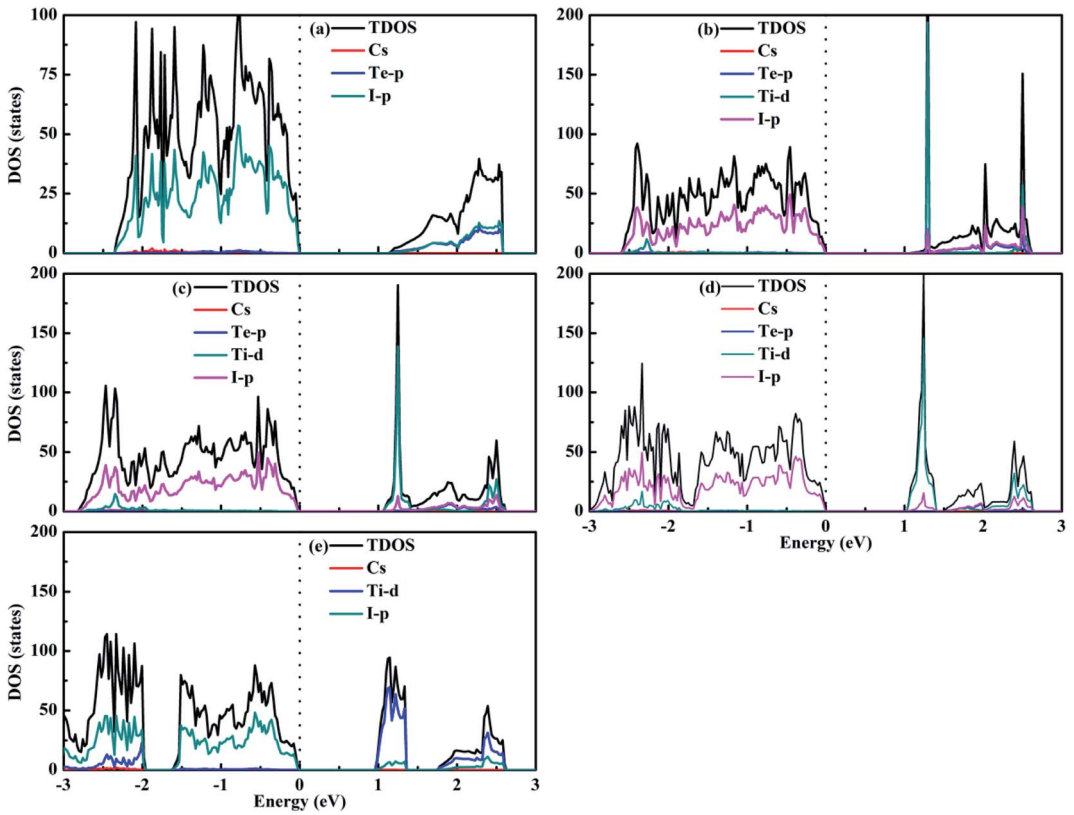

Fig. 7 Density of states of (a) Cs_2TeI_6, (b) $Cs_2Te_{0.75}Ti_{0.25}I_6$, (c) $Cs_2Te_{0.50}Ti_{0.50}I_6$, (d) $Cs_2Te_{0.25}Ti_{0.75}I_6$, and (e) Cs_2TiI_6.

 This journal is © The Royal Society of Chemistry 2020

Open Access Article. Published on 19 1442. Downloaded on 08/04/46 01:03:44 .
This article is licensed under a Creative Commons Attribution-NonCommercial 3.0 Unported Licence.

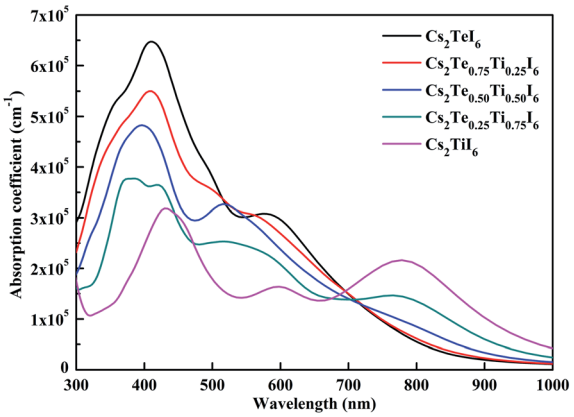

Fig. 8 The optical spectra of the $Cs_2Te_{1-x}Ti_xI_6$ solid solutions.

the conduction band minimum (CBM) is dominated by the Te-p orbitals along with the I-p orbitals. For Cs_2TiI_6, the VBM is mainly composed of the I-p orbitals, whereas the CBM is composed of the Ti-d orbitals. The similar situation is observed for the mixed Te–Ti double perovskites with respect to Cs_2TiI_6. It can be seen that Cs^+ does not contribute to the band edge states.

3.4 Optical properties

The calculated optical absorption spectrum is given in Fig. 8. Cs_2TeI_6 shows a large absorption coefficient in the visible light region. The absorption coefficient of Cs_2TiI_6 is over 10^{-5} cm^{-1} in the whole region, but it is lower than that of Cs_2TeI_6 in the range of 300–700 nm. For Cs_2TiI_6, two strong absorption peaks are located at about 450 and 800 nm, respectively. The optical absorption ability gradually increases when the proportion of Ti^{4+} decreases. In general, the $Cs_2Te_{1-x}Ti_xI_6$ solid solutions have strong and wide optical absorption in the visible spectrum. $Cs_2Te_{0.50}Ti_{0.50}I_6$ is the most promising candidate due to its superior stability, suitable direct band gap, and strong optical absorption.

4. Conclusions

In summary, the structural, mechanical, electronic and optical properties for the $Cs_2Te_{1-x}Ti_xI_6$ solid solutions have been investigated by using first-principles calculations for the first time. The calculated results show that Cs_2TeI_6 is an indirect band gap semiconductor, while Cs_2TiI_6 is a direct band gap semiconductor with the value of 0.98 eV. These compounds show good structural stability compared to $CH_3NH_3PbI_3$. An indirect–direct band gap transition can be observed when the doping concentration of Ti^{4+} is 0.50. $Cs_2Te_{0.50}Ti_{0.50}I_6$ has a suitable direct band gap (1.09 eV), which is considered as a promising photovoltaic material for single-junction solar cells. Further analysis reveals that all the structures are ductile materials except for $Cs_2Te_{0.50}Ti_{0.50}I_6$. Moreover, these materials have large optical absorption coefficients in the visible light region. We expect that this study can provide insights into developing the stable, non-toxic, and high-efficiency perovskite materials for optoelectronic devices.

Conflicts of interest

There are no conflicts to declare.

Acknowledgements

This work was supported by the National Natural Science Foundation of China (No. 21872033), the Department of Fujian Science and Technology and Program for Innovative Research Team in Science and Technology in Fujian Province University (No. 2018N2001), and the Fujian Key Laboratory of Functional Marine Sensing Materials (No. MJUKFFMSM201909). The authors thank the Supercomputer environment of Fujian Provincial Key Laboratory of Information Processing and Intelligent Control.

References

1 A. Kojima, K. Teshima, Y. Shirai and T. Miyasaka, *J. Am. Chem. Soc.*, 2009, **131**, 6050–6051.
2 W. S. Yang, B.-W. Park, E. H. Jung, N. J. Jeon, Y. C. Kim, D. U. Lee, S. S. Shin, J. Seo, E. K. Kim, J. H. Noh and S. I. Seok, *Science*, 2017, **356**, 1376–1379.
3 G. E. Eperon, T. Leijtens, K. A. Bush, R. Prasanna, T. Green, J. T.-W. Wang, D. P. McMeekin, G. Volonakis, R. L. Milot, R. May, A. Palmstrom, D. J. Slotcavage, R. A. Belisle, J. B. Patel, E. S. Parrott, R. J. Sutton, W. Ma, F. Moghadam, B. Conings, A. Babayigit, H.-G. Boyen, S. Bent, F. Giustino, L. M. Herz, M. B. Johnston, M. D. McGehee and H. J. Snaith, *Science*, 2016, **354**, 861–865.
4 NREL, *Photovoltaic Research. Best Research-Cell Efficiency Chart*, 2019, https://www.nrel.gov/pv/cell-efficiency.html.
5 N. K. Noel, S. D. Stranks, A. Abate, C. Wehrenfennig, S. Guarnera, A.-A. Haghighirad, A. Sadhanala, G. E. Eperon, S. K. Pathak, M. B. Johnston, A. Petrozza, L. M. Herz and H. J. Snaith, *Energy Environ. Sci.*, 2014, **7**, 3061–3068.
6 F. Hao, C. C. Stoumpos, D. H. Cao, R. P. H. Chang and M. G. Kanatzidis, *Nat. Photonics*, 2014, **8**, 489–494.
7 M. H. Kumar, S. Dharani, W. L. Leong, P. P. Boix, R. R. Prabhakar, T. Baikie, C. Shi, H. Ding, R. Ramesh, M. Asta, M. Graetzel, S. G. Mhaisalkar and N. Mathews, *Adv. Mater.*, 2014, **26**, 7122–7127.
8 T. Krishnamoorthy, H. Ding, C. Yan, W. L. Leong, T. Baikie, Z. Zhang, M. Sherburne, S. Li, M. Asta, N. Mathews and S. G. Mhaisalkar, *J. Mater. Chem. A*, 2015, **3**, 23829–23832.
9 C. C. Stoumpos, L. Frazer, D. J. Clark, Y. S. Kim, S. H. Rhim, A. J. Freeman, J. B. Ketterson, J. I. Jang and M. G. Kanatzidis, *J. Am. Chem. Soc.*, 2015, **137**, 6804–6819.
10 M.-G. Ju, G. Sun, Y. Zhao and W. Liang, *Phys. Chem. Chem. Phys.*, 2015, **17**, 17679–17687.
11 L.-J. Chen, *RSC Adv.*, 2018, **8**, 18396–18399.
12 B. Yang, J. Chen, F. Hong, X. Mao, K. Zheng, S. Yang, Y. Li, T. Pullerits, W. Deng and K. Han, *Angew. Chem., Int. Ed.*, 2017, **56**, 12471–12475.

Open Access Article. Published on 19 1442. Downloaded on 08/04/46 01:03:44.
This article is licensed under a Creative Commons Attribution-NonCommercial 3.0 Unported Licence.

13 J. Zhang, Y. Yang, H. Deng, U. Farooq, X. Yang, J. Khan, J. Tang and H. Song, *ACS Nano*, 2017, **11**, 9294–9302.
14 M. Leng, Y. Yang, K. Zeng, Z. Chen, Z. Tan, S. Li, J. Li, B. Xu, D. Li, M. P. Hautzinger, Y. Fu, T. Zhai, L. Xu, G. Niu, S. Jin and J. Tang, *Adv. Funct. Mater.*, 2018, **28**, 1704446.
15 Y. Lou, M. Fang, J. Chen and Y. Zhao, *Chem. Commun.*, 2018, **54**, 3779–3782.
16 J. Pal, A. Bhunia, S. Chakraborty, S. Manna, S. Das, A. Dewan, S. Datta and A. Nag, *J. Phys. Chem. C*, 2018, **122**, 10643–10649.
17 J. Pal, S. Manna, A. Mondal, S. Das, K. V. Adarsh and A. Nag, *Angew. Chem., Int. Ed.*, 2017, **56**, 14187–14191.
18 E. T. McClure, M. R. Ball, W. Windl and P. M. Woodward, *Chem. Mater.*, 2016, **28**, 1348–1354.
19 F. Wei, Z. Deng, S. Sun, F. Xie, G. Kieslich, D. M. Evans, M. A. Carpenter, P. D. Bristowe and A. K. Cheetham, *Mater. Horiz.*, 2016, **3**, 328–332.
20 G. Volonakis, A. A. Haghighirad, R. L. Milot, W. H. Sio, M. R. Filip, B. Wenger, M. B. Johnston, L. M. Herz, H. J. Snaith and F. Giustino, *J. Phys. Chem. Lett.*, 2017, **8**, 772–778.
21 P. Cheng, T. Wu, Y. Li, L. Jiang, W. Deng and K. Han, *New J. Chem.*, 2017, **41**, 9598–9601.
22 C. Zhang, L. Gao, S. Teo, Z. Guo, Z. Xu, S. Zhao and T. Ma, *Sustainable Energy Fuels*, 2018, **2**, 2419–2428.
23 C. C. Stoumpos, C. D. Malliakas and M. G. Kanatzidis, *Inorg. Chem.*, 2013, **52**, 9019–9038.
24 A. H. Slavney, T. Hu, A. M. Lindenberg and H. I. Karunadasa, *J. Am. Chem. Soc.*, 2016, **138**, 2138–2141.
25 H. Lin, C. Zhou, Y. Tian, T. Siegrist and B. Ma, *ACS Energy Lett.*, 2018, **3**, 54–62.
26 X. Qiu, B. Cao, S. Yuan, X. Chen, Z. Qiu, Y. Jiang, Q. Ye, H. Wang, H. Zeng, J. Liu and M. G. Kanatzidis, *Sol. Energy Mater. Sol. Cells*, 2017, **159**, 227–234.
27 M. Rasukkannu, D. Velauthapillai and P. Vajeeston, *Mater. Lett.*, 2018, **218**, 233–236.
28 F. Funabiki, Y. Toda and H. Hosono, *J. Phys. Chem. C*, 2018, **122**, 10749–10754.
29 A. E. Maughan, A. M. Ganose, M. M. Bordelon, E. M. Miller, D. O. Scanlon and J. R. Neilson, *J. Am. Chem. Soc.*, 2016, **138**, 8453–8464.
30 M.-G. Ju, M. Chen, Y. Zhou, H. F. Garces, J. Dai, L. Ma, N. P. Padture and X. C. Zeng, *ACS Energy Lett.*, 2018, **3**, 297–304.
31 N. Hernández-Haro, J. Ortega-Castro, Y. B. Martynov, R. G. Nazmitdinov and A. Frontera, *Chem. Phys.*, 2019, **516**, 225–231.
32 K. Chakraborty, M. G. Choudhury and S. Paul, *Sol. Energy*, 2019, **194**, 886–892.
33 H. Yan, Y. Li, X. Li, B. Wang and M. Li, *RSC Adv.*, 2020, **10**, 958–964.
34 M. Tsuyama and S. Suzuki, *J. Phys. Soc. Jpn.*, 2019, **88**, 104802.
35 M. Chen, M.-G. Ju, A. D. Carl, Y. Zong, R. L. Grimm, J. Gu, X. C. Zeng, Y. Zhou and N. P. Padture, *Joule*, 2018, **2**, 558–570.
36 L. Zhou, J.-F. Liao, Z.-G. Huang, X.-D. Wang, Y.-F. Xu, H.-Y. Chen, D.-B. Kuang and C.-Y. Su, *ACS Energy Lett.*, 2018, **3**, 2613–2619.
37 D. Ju, X. Zheng, J. Yin, Z. Qiu, B. Türedi, X. Liu, Y. Dang, B. Cao, O. F. Mohammed, O. M. Bakr and X. Tao, *ACS Energy Lett.*, 2019, **4**, 228–234.
38 D. Liu, Q. Li, Z. Zhang and K. Wu, *New J. Chem.*, 2019, **43**, 14892–14897.
39 G. Kresse and J. Furthmüller, *Comput. Mater. Sci.*, 1996, **6**, 15–50.
40 P. E. Blöchl, *Phys. Rev. B: Condens. Matter Mater. Phys.*, 1994, **50**, 17953–17979.
41 J. P. Perdew, K. Burke and M. Ernzerhof, *Phys. Rev. Lett.*, 1996, **77**, 3865–3868.
42 T. Thonhauser, V. R. Cooper, S. Li, A. Puzder, P. Hyldgaard and D. C. Langreth, *Phys. Rev. B: Condens. Matter Mater. Phys.*, 2007, **76**, 125112.
43 E. Finazzi, C. Di Valentin, G. Pacchioni and A. Selloni, *J. Chem. Phys.*, 2008, **129**, 154113.
44 H. J. Snaith, *J. Phys. Chem. Lett.*, 2013, **4**, 3623–3630.
45 Y. Zhao and K. Zhu, *Chem. Soc. Rev.*, 2016, **45**, 655–689.
46 R. Ali, G.-J. Hou, Z.-G. Zhu, Q.-B. Yan, Q.-R. Zheng and G. Su, *Chem. Mater.*, 2018, **30**, 718–728.
47 O. Hellman, I. A. Abrikosov and S. I. Simak, *Phys. Rev. B: Condens. Matter Mater. Phys.*, 2011, **84**, 180301.
48 F. D. Murnaghan, *Am. J. Math.*, 1937, **59**, 235–260.
49 M. Born, *Math. Proc. Cambridge Philos. Soc.*, 2008, **36**, 160–172.
50 R. Hill, *Proc. Phys. Soc.*, 1952, **65**, 349–354.
51 M. Roknuzzaman, K. Ostrikov, H. Wang, A. Du and T. Tesfamichael, *Sci. Rep.*, 2017, **7**, 14025.
52 S. F. Pugh, *London, Edinburgh Dublin Philos. Mag. J. Sci.*, 1954, **45**, 823–843.
53 M. A. Hadi, M. Roknuzzaman, A. Chroneos, S. H. Naqib, A. K. M. A. Islam, R. V. Vovk and K. Ostrikov, *Comput. Mater. Sci.*, 2017, **137**, 318–326.
54 E. Y. Peresh, V. I. Sidei, N. I. Gaborets, O. V. Zubaka, I. P. Stercho and I. E. Barchii, *Inorg. Mater.*, 2014, **50**, 101–106.
55 E. Y. Peresh, O. V. Zubaka, V. I. Sidei, I. E. Barchii, S. V. Kun and A. V. Kun, *Inorg. Mater.*, 2002, **38**, 859–863.
56 W. Shockley and H. J. Queisser, *J. Appl. Phys.*, 1961, **32**, 510–519.

This journal is © The Royal Society of Chemistry 2020